



# CHORUS

This is the accepted manuscript made available via CHORUS. The article has been published as:

## Nonlinear Sideband Cooling to a Cat State of Motion

B. D. Hauer, J. Combes, and J. D. Teufel

Phys. Rev. Lett. **130**, 213604 — Published 25 May 2023

DOI: [10.1103/PhysRevLett.130.213604](https://doi.org/10.1103/PhysRevLett.130.213604)

# Nonlinear Sideband Cooling to a Cat State of Motion

B.D. Hauer,<sup>1,\*</sup> J. Combes,<sup>2</sup> and J.D. Teufel<sup>1,†</sup>

<sup>1</sup>*National Institute of Standards and Technology, Boulder, Colorado 80305, USA*

<sup>2</sup>*Department of Electrical, Computer, and Energy Engineering,  
University of Colorado, Boulder, Colorado 80309, USA*

(Dated: March 15, 2023)

The ability to prepare a macroscopic mechanical resonator into a quantum superposition state is an outstanding goal of cavity optomechanics. Here we propose a technique to generate cat states of motion using the intrinsic nonlinearity of a dispersive optomechanical interaction. By applying a bichromatic drive to an optomechanical cavity, our protocol enhances the inherent second-order processes of the system, inducing the requisite two-phonon dissipation. We show that this nonlinear sideband cooling technique can dissipatively engineer a mechanical resonator into a cat state, which we verify using the full Hamiltonian and an adiabatically reduced model. While the fidelity of the cat state is maximized in the single-photon, strong-coupling regime, we demonstrate that Wigner negativity persists even for weak coupling. Finally, we show that our cat state generation protocol is robust to significant thermal decoherence of the mechanical mode, indicating that such a procedure may be feasible for near-term experimental systems.

*Introduction*—Engineered micro/nanomechanical systems have recently emerged as viable resources for quantum technologies [1] and fundamental tests of quantum mechanics [2]. At the forefront of this effort is cavity optomechanics [3], which utilizes sideband techniques to stabilize quantum states of motion via reservoir engineering [4]. Canonical examples include ground state cooling [5, 6], squeezing [7, 8], and entanglement [9–12] of mechanical motion. However, these protocols rely on a strong pump to parametrically enhance the linear coupling between the cavity field and mechanical motion, obscuring the inherent nonlinearity of the interaction. Thus the current field of quantum optomechanics is largely confined to performing bilinear operations on Gaussian states. By reinforcing the intrinsic optomechanical nonlinearity, one could break free of this Gaussian prison and prepare interesting non-classical states of mechanical motion.

Of particular interest are macroscopic superposition states known as cat states [13], which have previously been observed in trapped ions [14], confined photons [15], and superconducting circuits [16, 17]. Though recent experiments have prepared non-Gaussian states of mechanical motion using nonlinearities derived from superconducting qubits [18–21] and single-photon detection [10, 22, 23], the experimental generation of macroscopic superposition states has yet to be demonstrated. Preparing these highly non-classical states in mechanical resonators would allow them to be used as quantum-enhanced sensors [24–26], nodes in quantum communication networks [27, 28], long-lived, error-protected qubits [29, 30], and platforms to study macroscopic quantum collapse theories [31].

Early proposals to create mechanical cat states utilized the intrinsic Kerr nonlinearity of the optomechanical interaction [31, 32], however, this method requires vacuum coupling larger than both the mechanical frequency and cavity loss rate. Subsequent optomechanical cat state generation protocols have suggested introducing nonlinearities via single-photon detection to perform conditional measurements [33, 34] or single-phonon addition/subtraction [35, 36], cou-

pling with external two-level systems [37, 38], swaps between non-classical cavity states and mechanical modes [39, 40], or using time-varying electromagnetic fields [41–45]. Each of these proposals rely on some combination of probabilistic measurements, complicated integration with external sources of nonlinearity (*e.g.* qubits), and/or generation of complex electromagnetic fields. Beyond being difficult to implement experimentally, the complexity of these methods will incur inefficiencies in the mechanical cat state preparation, decreasing its fidelity. On the other hand, optomechanical protocols that utilize reservoir engineering techniques [4] have recently been proposed for the deterministic and stable generation of macroscopic mechanical superposition states [46–49]. Such schemes utilize continuous, coherent electromagnetic sources and are robust to external decoherence. Unfortunately, these proposed methods have relied on quadratic coupling between the cavity and mechanical element, which is small relative to its destructive linear counterpart [50, 51].

Here, we introduce a reservoir engineering technique that uses the nonlinearity inherent to all optomechanical systems to prepare cat states of motion. This simple scheme differentiates itself from previous reservoir engineering proposals, as it circumvents the experimentally prohibitive requirement for direct coupling to the square of mechanical displacement. Furthermore, our technique obviates the need for external sources of nonlinearity or complex electromagnetic drives, providing a resource-efficient method to generate macroscopic superposition states. For this protocol, one applies two continuous-wave pumps to an optomechanical cavity, one resonant and one red-detuned by twice the mechanical frequency. This prepares the mechanical resonator into a cat state via two-phonon sideband cooling and squeezing processes. Using a master equation approach, we deduce that mechanical cat state generation is feasible for vacuum coupling rates that are greater than the cavity loss rate, but much smaller than the mechanical frequency. By numerically simulating the full optomechanical Hamiltonian, we verify that our protocol can generate high-fidelity mechanical cat states

with near ideal Wigner negativity. Finally, we show that our protocol is robust to contamination from the surrounding environment, allowing for preparation of mechanical superposition states in the presence of thermal noise.

*Dissipation Engineering Protocol*—Our procedure is adapted from a previous technique used to prepare cat states in superconducting microwave cavities coupled via a Josephson nonlinearity [16, 17]. In this protocol, the cat state is prepared in the long-lived “storage” cavity, while a second “readout” cavity is used to engineer nonlinear dissipation processes. This protocol naturally maps to an optomechanical system, whereby the mechanical resonator becomes the “storage” element, with the coupled electromagnetic cavity providing the fast “readout”. The requisite nonlinearity is then provided by the optomechanical interaction itself in place of a Josephson junction. With this architecture, one can apply a strong pump to the cavity red-detuned by twice the mechanical frequency to mediate two-phonon cooling processes (see Fig. 1). A second tone applied on resonance will then mix with this detuned pump providing a two-phonon mechanical drive. Combined, these two-phonon processes are parity preserving, such that a resonator initialized into an even (odd) state will be restricted to the even (odd) manifold of its Fock basis and will evolve into an even (odd) cat state [46]. Along with these nonlinear processes, linear optomechanical coupling will persist in any realistic system, acting to flip the parity of the desired cat state and contribute to its decoherence [52]. Therefore, we must treat the optomechanical Hamiltonian in its entirety, such that both linear and nonlinear terms are included.

To investigate our protocol, we begin with the optomechanical master equation

$$\dot{\rho} = -\frac{i}{\hbar}[H, \rho] + \kappa L[a]\rho + \Gamma(\bar{n}_b + 1)L[b]\rho + \Gamma\bar{n}_b L[b^\dagger]\rho, \quad (1)$$

where  $a$  ( $b$ ) is the annihilation operator for the electromagnetic cavity (mechanical resonator). Here we assume a zero temperature bath for the cavity (*i.e.*  $\bar{n}_a = 0$ ) with total loss rate  $\kappa$  and frequency  $\omega_c$ . Meanwhile, the mechanical mode with frequency  $\omega_m$  is thermalized at its decay rate  $\Gamma$  to an environment at finite temperature  $T$  and average occupancy  $\bar{n}_b = (e^{\hbar\omega_m/k_B T} - 1)^{-1}$ . We have also introduced the Lindblad superoperator  $L[o]\rho = o^\dagger o \rho - \frac{1}{2}o^\dagger o \rho - \frac{1}{2}\rho o^\dagger o$  for arbitrary operator  $o$  and density matrix  $\rho$ , as well as the optomechanical Hamiltonian in the frame rotating at the pump frequency  $\omega_p$

$$\begin{aligned} \frac{H}{\hbar} = & -\Delta a^\dagger a + \omega_m b^\dagger b + \varepsilon_d a^\dagger e^{i\Delta_p t} + \varepsilon_d^* a e^{-i\Delta_p t} \\ & + (g_1^* a + g_1 a^\dagger)(b + b^\dagger) + g_0 a^\dagger a (b + b^\dagger). \end{aligned} \quad (2)$$

Here we have translated the cavity mode by its steady state amplitude  $\alpha = \varepsilon_p / (\Delta + i\kappa/2)$  in the presence of a coherent pump with amplitude  $\varepsilon_p$ , where  $\Delta = \omega_p - \omega_c$ , such that  $a$  now acts on the displaced cavity mode. The average number of photons in the cavity due to this pump can be calculated as  $\bar{n}_p = |\alpha|^2$ . Note that in Eq. (2) we have implicitly accounted

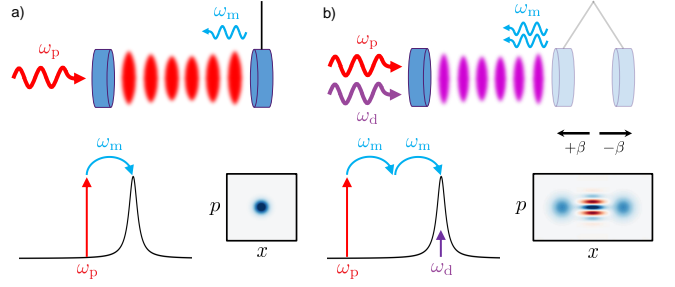


FIG. 1: Schematic, frequency-space, and phase-space representations of a) conventional optomechanical sideband cooling and b) our proposed method of mechanical cat state generation using nonlinear sideband cooling.

for the static displacement in mechanical equilibrium position due to this steady state photon population, as well as the corresponding shift in cavity frequency, by appropriately modifying our reference frame [53]. Also included is a coherent cavity drive with amplitude  $\varepsilon_d$  and frequency  $\omega_d$  detuned from the pump frequency by  $\Delta_p = \omega_p - \omega_d$ . Finally, the last two terms in Eq. (2) characterize the linearized and nonlinear optomechanical interactions, with the linear cavity-enhanced coupling rate  $g_1 = \alpha g_0$  expressed in terms of the optomechanical vacuum coupling rate  $g_0$ .

While Eq. (2) gives an exact description of our optomechanical cavity, often the final term is neglected, leading to a linearized description. However, this term is crucial in providing the nonlinearity required for our protocol. We therefore use a Schrieffer-Wolff transformation [68] with the generator  $S = \frac{g_0}{\omega_m} a^\dagger a (b^\dagger - b)$  [69] to expand this term to leading order in  $g_0/\omega_m$ , which amounts to the replacement [53]

$$\begin{aligned} g_0 a^\dagger a (b + b^\dagger) \Rightarrow & (g_2^* a - g_2 a^\dagger) (b^2 - b^{\dagger 2}) \\ & - \frac{g_0^2}{\omega_m} \left\{ (a^\dagger a)^2 + \alpha^* (2a^\dagger a + 1) a + \alpha a^\dagger (2a^\dagger a + 1) \right\}. \end{aligned} \quad (3)$$

The first term in Eq. (3) elucidates the fact that the intrinsic optomechanical nonlinearity can be used to mediate second-order processes whereby single photons simultaneously interact with two phonons at a strength determined by the second-order coupling rate  $g_2 = g_0^2 \alpha / \omega_m$ . Meanwhile the second term corresponds to the higher-order corrections to the electromagnetic cavity in the presence of optomechanical coupling, including the well-known self-Kerr nonlinearity [3].

*Adiabatically Eliminated Model*—To proceed, we assume that the cavity’s decay rate  $\kappa$  exceeds the interaction rates of the mechanical resonator with its thermal bath and the electromagnetic cavity [53]. In this regime, the system will quickly equilibrate to its steady state, which we take to be the slow subspace spanned by the cavity’s ground state and the full Hilbert space of the mechanical mode. We then adiabatically eliminate the cavity mode by tracing over its rapidly evolving excited states. This is performed using the Nakajima-Zwanzig formalism [70] to derive the reduced master equation for the mechanical mode in the sideband-resolved regime ( $\kappa \ll \omega_m$ )

as

$$\dot{\rho}_b = -\frac{i}{\hbar}[H_b, \rho_b] + \Gamma_2 L[b^2]\rho_b + \Gamma_{\text{lin}} L[b]\rho_b + \Gamma_{\text{ex}} L[b^\dagger]\rho_b, \quad (4)$$

where

$$\frac{H_b}{\hbar} = \varepsilon_2 b^{\dagger 2} + \varepsilon_2^* b^2 - K (b^\dagger b)^2. \quad (5)$$

Here we have chosen to maximize cat state generation efficiency by applying the drive tone on resonance with the cavity ( $\omega_d = \omega_c$ ) and the pump tone at  $\omega_p = \omega_c - 2\tilde{\omega}_m$ , where  $\tilde{\omega}_m$  is the dressed mechanical frequency [53].

Eq. (4) includes all of the terms necessary to dissipatively engineer mechanical cat states. The first term describes the evolution of the resonator according to  $H_b$ . This Hamiltonian contains coherent two-phonon squeezing terms, with amplitude  $\varepsilon_2 = 2i\varepsilon_d g_2^*/\kappa$ , that arise from the mixing of the pump tones applied to the cavity, along with a phonon-dependent Kerr nonlinearity with strength  $K = |g_2|^2/4\omega_m$ . The second term describes two-phonon optomechanical cooling at a rate  $\Gamma_2 = 4|g_2|^2/\kappa$ . This engineered cooling, coupled with the squeezing terms, restricts the mechanical resonator to two-phonon operations, thus preserving its parity. Acting under these two processes alone, the resonator will naturally evolve from the ground state into an even cat state on a timescale set by  $\tau \sim 1/\Gamma_2$  (see Fig. 2). The size of the resultant cat state is given by  $\beta = \sqrt{|\varepsilon_d|/|g_2|}$ , while its rotation in phase space is set by the relative phase between  $\varepsilon_p$  and  $\varepsilon_d$ .

Meanwhile, the last two terms in Eq. (4) represent incoherent single-phonon loss and excitation processes. In the first case, decoherence is caused by the mechanical resonator emitting phonons at a rate  $\Gamma_{\text{lin}} = \Gamma_{\text{th}} + \Gamma_1$  into either to its intrinsic environmental bath at its thermal decoherence rate  $\Gamma_{\text{th}} = (\bar{n}_b + 1)\Gamma$ , or to an optomechanically generated reservoir at rate  $\Gamma_1 = |g_1|^2 \kappa / \omega_m^2$ . The term proportional to  $L[b^\dagger]\rho_b$  then corresponds to incoherent phononic excitations from these two baths at a rate  $\Gamma_{\text{ex}} = \bar{n}_b \Gamma + \Gamma_1/9$ . Both of these single-phonon processes will flip the parity of the cat state from even to odd (or vice versa), causing it to decohere at a rate  $\Gamma_{\text{dec}} = 2|\beta|^2(\Gamma_{\text{lin}} + \Gamma_{\text{ex}})$  [52]. To generate mechanical cat states we require  $\Gamma_{\text{lin}} \gg \Gamma_{\text{ex}}$ , so here we will focus on  $\Gamma_{\text{lin}}$ . However, we retain the incoherent excitation terms in our numerical analysis, as they will have noticeable effects on the cat state's coherence. Simulations using Eq. (4) can be seen in Fig. 2b, where we show the evolution of the mechanical resonator from its ground state into an even cat state of size  $\beta = 2$ .

In the ideal situation where  $\Gamma_{\text{th}} \ll \Gamma_1$ , only optomechanically induced losses need be considered, which sets a fundamental limit on our protocol's ability to generate mechanical cat states as  $\Gamma_2 \gtrsim \Gamma_1$ , or equivalently,

$$g_0 \gtrsim \frac{\kappa}{2}. \quad (6)$$

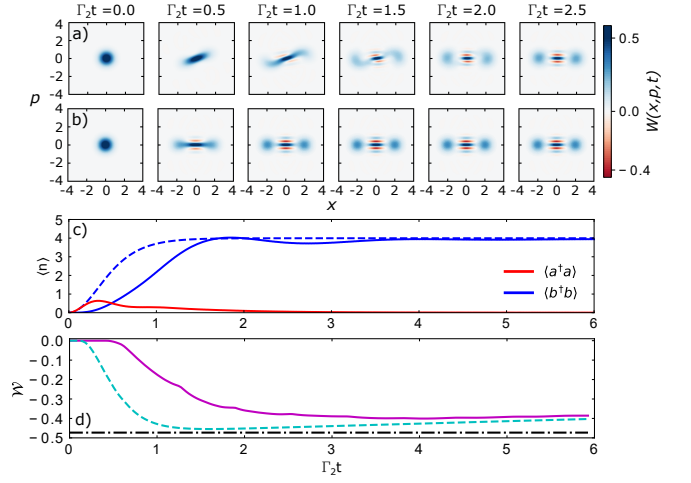


FIG. 2: Evolution of a mechanical resonator's Wigner distribution from its ground state to a  $\beta = 2$  even cat state using our reservoir engineering protocol simulated with a) the full master equation in Eq. (1) and b) the reduced master equation in Eq. (4). We also show c) the average occupancy of the mechanical and cavity modes and d) the minimal Wigner negativity of the mechanical state vs evolution time (full model - solid, reduced model - dashed). Simulation parameters are given in the main text. Here we find that for the full (reduced) model the Wigner negativity is minimized to  $\mathcal{W}_{\text{min}} = -0.401$  ( $\mathcal{W}_{\text{min}} = -0.455$ ) at  $\Gamma_2 t \approx 3.9$  ( $\Gamma_2 t \approx 1.6$ ). This corresponds to a maximal fidelity of 95.6% (99.1%) with an ideal even cat state of the same size, whose minimal Wigner negativity ( $\mathcal{W}_+ \approx -0.476$ ) is indicated by the black dashed-dotted line in d).

That is, the protocol outlined in this paper is optimal when the vacuum coupling rate of the system is on the order of, or exceeds, the loss rate of the cavity (*i.e.* approaching or residing in the single-photon, strong-coupling regime). We also note that for  $\beta \geq 1$ , Eq. (6) ensures that the autonomously stabilized cat states generated by our protocol can be used in error correction protocols where single quanta loss is the dominant error channel [17].

**Wigner Negativity**—To rigorously characterize the quantum superposition states generated using our procedure, we use the Wigner function  $W(x,p)$ , whose minimum we label the Wigner negativity or  $\mathcal{W} = \min\{W(x,p)\}$  [53]. For dynamic systems,  $\mathcal{W}$  can be further minimized in time, resulting in the minimal Wigner negativity  $\mathcal{W}_{\text{min}}$ . Using a phenomenological model, we show that for  $\Gamma_{\text{th}} \ll \Gamma_1$  the minimal Wigner negativity for our dissipation engineering protocol takes the simple form [53]

$$\mathcal{W}_{\text{min}} = \mathcal{W}_+ \exp \left[ -2C|\beta|^2 \left( \frac{\kappa}{2g_0} \right)^{2k+2} \right]. \quad (7)$$

Here  $C$  and  $k$  are parameters that characterize the time required to reach this minimal Wigner negativity as

$$t_{\text{min}} = \frac{C}{\Gamma_2} \left( \frac{\Gamma_1}{\Gamma_2} \right)^k, \quad (8)$$

while  $\mathcal{W}_+$  is the Wigner negativity of an ideal even cat state.

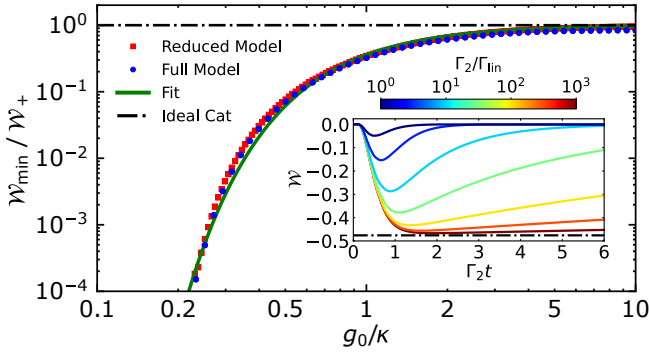


FIG. 3:  $\mathcal{W}_{\min}$  (normalized by  $\mathcal{W}_+ = 0.476$ ) versus  $g_0/\kappa$  for the same parameters as Fig. 2 with varying  $\kappa$  and  $\beta = 2$ . Here we observe excellent agreement between the full (blue circles) and reduced (red squares) optomechanical models over nearly two orders of magnitude in  $g_0/\kappa$ . Furthermore, the Wigner negativity approaches  $\mathcal{W}_+$  (black dashed-dotted line) for  $g_0/\kappa \gg 1/2$ , while exponentially decreasing for  $g_0/\kappa < 1/2$  as expected. Also included is a fit of Eq. (7) to the full model (solid green line). Inset:  $\mathcal{W}$  versus time for varying ratios of  $\Gamma_2/\Gamma_{\text{lin}}$ . Here we have chosen  $\kappa/2\pi = 10$  kHz, such that  $g_0/\kappa = 100$ , while varying  $\Gamma$ .

From Eq. (7), one can see that while Eq. (6) sets the scale for mechanical cat state generation, it is a soft limit, as non-zero Wigner negativity persists for  $2g_0 < \kappa$ . However, far below this limit the Wigner negativity dies off exponentially as a function of  $\kappa/2g_0$  (see Fig. 3).

*Numerical Simulations*—Using a numerical approach, we verify our model given in Eq. (4) against the full optomechanical model of Eq. (1). This is shown in Fig. 2, where we compare the evolution of a mechanical system from its ground state to a cat state using both models. Simulations are performed with the shared parameters  $g_0/2\pi = 1$  MHz,  $\omega_m/2\pi = 15$  MHz,  $\Gamma/2\pi = 15$  Hz,  $\kappa/2\pi = 100$  kHz,  $\bar{n}_b = 0$ , and  $\bar{n}_p = 0.1$ , with  $\varepsilon_d$  chosen such that  $\beta = 2$ . This parameter set allows for fast simulation, and hence a concrete comparison between these two models. Though they differ at earlier times, both models agree well on long timescales where  $\langle a^\dagger a \rangle \approx 0$  and the cat state has stabilized, thus validating our adiabatically eliminated model.

We have also assessed how the condition in Eq. (6) affects the minimal Wigner negativity of our generated cat states. This is presented in Fig. 3 using the same parameters as Fig. 2, while changing  $\kappa$  to vary the ratio  $g_0/\kappa$ . We find that Eq. (7) provides an excellent fit of the exact numerical results over multiple orders of magnitude in  $g_0/\kappa$  with the parameters  $C \approx 1/3$  and  $k \approx -1/4$ . This indicates that the minimal Wigner negativity of the  $\beta = 2$  cat state studied here decays exponentially in proportion to  $|\beta|^2 (\kappa/2g_0)^{3/2}$ . In spite of this exponential behavior, significant Wigner negativity still persists for  $g_0/\kappa \lesssim 0.3$ . Conversely, when  $g_0 \gg \kappa$ , the minimal Wigner negativity extracted from both models asymptotically approach their ideal values and high-fidelity cat states are created. We have additionally investigated the effect of increasing the mechanical decoherence rate  $\Gamma_{\text{lin}}$  on

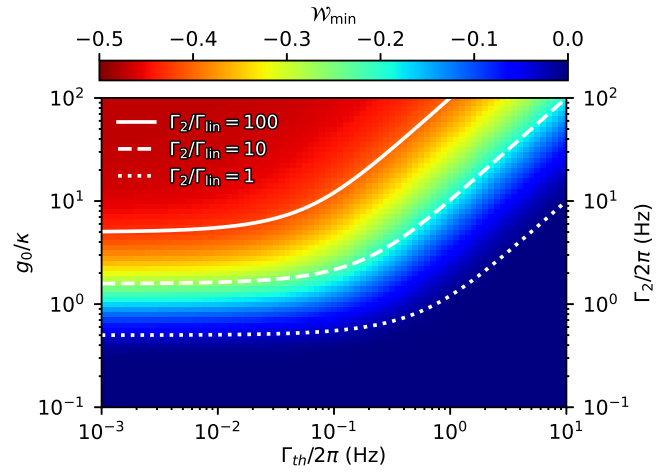


FIG. 4: Plot of  $\mathcal{W}_{\min}$  versus  $g_0/\kappa$  and  $\Gamma_{\text{th}}$  calculated using the reduced model in Eq. (4). Here we have fixed  $g_0/2\pi = 10$  kHz,  $\omega_m/2\pi = 20$  MHz,  $\bar{n}_b = 10$  (corresponding to  $T \approx 10$  mK), and  $\bar{n}_p = 100$ , while  $\kappa$  and  $\Gamma$  are swept to vary  $g_0/\kappa$  (or equivalently  $\Gamma_2$ ) and  $\Gamma_{\text{th}}$ , respectively. We have also chosen  $\varepsilon_d$  such that the generated cat state is of size  $\beta = 2$  at every point in the plot.

the time-dependence of the cat state's Wigner negativity (inset of Fig. 3). Here we confirm that the Wigner negativity is minimized on a timescale set by  $1/\Gamma_2$ , with a weak dependence on  $\Gamma_1/\Gamma_2$  as indicated by Eq. (8). We further observe the minimal Wigner negativity approaches  $\mathcal{W}_+$  for  $\Gamma_2/\Gamma_{\text{lin}} \gg 1$ , while decohering back to zero on a timescale set by  $1/\Gamma_{\text{lin}}$ .

Finally, we have used our adiabatically eliminated model to investigate how  $\mathcal{W}_{\min}$  varies over a large parameter space in  $g_0/\kappa$  and  $\Gamma_{\text{th}}$ , which is illustrated in Fig. 4. On the right side of the plot where  $\Gamma_{\text{lin}} \approx \Gamma_{\text{th}}$ , regions of significant Wigner negativity are delineated by contours that exhibit a linear dependence between  $g_0/\kappa$  and  $\Gamma_{\text{th}}$ . Meanwhile on the left side, these boundaries plateau to a constant value. This is because the decoherence is no longer dominated by the thermal environment, but instead by pump-induced linear dissipation. As  $\Gamma_1$  and  $\Gamma_2$  scale with pump power in the same way, their ratio is constant and given by  $(2g_0/\kappa)^2$  [53]. These results show clearly demarcated regions of parameters space that allow for significant Wigner negativity even in the presence of significant thermal noise.

*Experimental Realization*—Currently, the most challenging aspect of experimentally realizing our protocol is the condition given by Eq. (6). While existing experiments in microwave circuits [71] and optomechanical crystals [72] have demonstrated  $2g_0/\kappa \approx 0.01$ , ongoing improvements in both coupling and cavity losses make each of these platforms a viable candidate for achieving  $2g_0/\kappa \approx 1$ . Specifically, in optomechanical crystals, numerical optimization of ultra-small mode volume cavities projects to increase the vacuum coupling, while ensuring that radiation and fabrication uniformity do not limit the cavity losses [73]. In the microwave regime, bulk superconducting cavities already achieve sufficiently low loss [74] and ongoing advances in materials and

surface preparation could allow similar quality factors in vacuum gap capacitor optomechanical circuits. In addition to improvements in loss, recent proposals suggest that by pushing circuit optomechanics into the millimeter-wave regime,  $g_0$  could also be increased by over an order of magnitude [75]. Together these innovations in increased coupling and cavity quality factor would enable experimental implementation of this cat state protocol. Regardless of the platform, verification of these delicate quantum superposition states will require the ability to perform mechanical state tomography with low added noise. Conveniently, cavity optomechanical systems have demonstrated nearly noiseless mechanical quadrature measurement techniques, using either quantum nondemolition [8] or transient amplification [76] methods, which are sufficient for witnessing Wigner negativity.

*Conclusion*—We have introduced a simple scheme that utilizes two continuous-wave pumps to cool an optomechanical resonator into a cat state of motion. To generate significant Wigner negativity with such a protocol, one must approach the single-photon, strong coupling regime. Though unattainable in current experiments, with future improvements to state-of-the-art optomechanical systems, mechanical cat state generation using this protocol could soon be realized. This advancement would allow for straightforward preparation of long-lived mechanical cat states to be used as robust, rotation-symmetric bosonic codes for quantum computing [77], or as canonical systems to study the fundamental collapse mechanisms of macroscopic quantum superposition states [31].

The authors would like to thank Matthew Woolley for fruitful discussions, as well as Scott Glancy and Nicholas Frattini for their careful reading of the manuscript and insightful comments. JC was supported in part by NSF QLCI Award No. OMA-2016244. BDH acknowledges financial support from NSERC and Banting postdoctoral fellowships. Contributions to this article by workers at NIST, an agency of the U.S. Government, are not subject to U.S. copyright.

---

\* Electronic address: bradley.hauer@nist.gov

† Electronic address: john.teufel@nist.gov

- [1] S. Barzanjeh, A. Xuereb, S. Gröblacher, M. Paternostro, C. A. Regal, and E. M. Weig, *Nat. Phys.* **18**, 15 (2022).
- [2] Y. Chen, *J. Phys. B* **46**, 104001 (2013).
- [3] M. Aspelmeyer, T. J. Kippenberg, and F. Marquardt, *Rev. Mod. Phys.* **86**, 1391 (2014).
- [4] J. F. Poyatos, J. I. Cirac, and P. Zoller, *Phys. Rev. Lett.* **77**, 4728 (1996).
- [5] J. D. Teufel, T. Donner, D. Li, J. W. Harlow, M. S. Allman, K. Cicak, A. J. Sirois, J. D. Whittaker, K. W. Lehnert, and R. W. Simmonds, *Nature* **475**, 359 (2011).
- [6] J. Chan, T. P. M. Alegre, A. H. Safavi-Naeini, J. T. Hill, A. Krause, S. Gröblacher, M. Aspelmeyer, and O. Painter, *Nature* **478**, 89 (2011).
- [7] E. E. Wollman, C. U. Lei, A. J. Weinstein, J. Suh, A. Kronwald, F. Marquardt, A. A. Clerk, and K. C. Schwab, *Science* **349**, 952 (2015).
- [8] F. Lecocq, J. B. Clark, R. W. Simmonds, J. Aumentado, and J. D. Teufel, *Phys. Rev. X* **5**, 041037 (2015).
- [9] T. A. Palomaki, J. D. Teufel, R. W. Simmonds, and K. W. Lehnert, *Science* **342**, 710 (2013).
- [10] R. Riedinger, A. Wallucks, I. Marinković, C. Lössnauer, M. Aspelmeyer, S. Hong, and S. Gröblacher, *Nature* **556**, 473 (2018).
- [11] C. F. Ockeloen-Korppi, E. Damskägg, J.-M. Pirkkalainen, M. Asjad, A. A. Clerk, F. Massel, M. J. Woolley, and M. A. Sillanpää, *Nature* **556**, 478 (2018).
- [12] S. Kotler, G. A. Peterson, E. Shojaei, F. Lecocq, K. Cicak, A. Kwiatkowski, S. Geller, S. Glancy, E. Knill, R. W. Simmonds, J. Aumentado, and J. D. Teufel, *Science* **372**, 622 (2021).
- [13] E. Schrödinger, *Naturwissenschaften* **23**, 807 (1935).
- [14] C. Monroe, D. M. Meekhof, B. E. King, and D. J. Wineland, *Science* **272**, 1131 (1996).
- [15] M. Brune, E. Hagley, J. Dreyer, X. Maître, A. Maali, C. Wunderlich, J. M. Raimond, and S. Haroche, *Phys. Rev. Lett.* **77**, 4887 (1996).
- [16] Z. Leghtas, S. Touzard, I. M. Pop, A. Kou, B. Vlastakis, A. Petrenko, K. M. Sliwa, A. Narla, S. Shankar, M. J. Hatridge, M. Reagor, L. Frunzio, R. J. Schoelkopf, M. Mirrahimi, and M. H. Devoret, *Science* **347**, 853 (2015).
- [17] R. Lescanne, M. Villiers, T. Peronnin, A. Sarlette, M. Delbecq, B. Huard, T. Kontos, M. Mirrahimi, and Z. Leghtas, *Nat. Phys.* **16**, 509 (2020).
- [18] A. D. O’Connell, M. Hofheinz, M. Ansmann, R. C. Bialczak, M. Lenander, E. Lucero, M. Neeley, D. Sank, H. Wang, M. Weides, J. Wenner, J. M. Martinis, and A. N. Cleland, *Nature* **464**, 697 (2010).
- [19] Y. Chu, P. Kharel, T. Yoon, L. Frunzio, P. T. Rakich, and R. J. Schoelkopf, *Nature* **563**, 666 (2018).
- [20] X. Ma, J. J. Viennot, S. Kotler, J. D. Teufel, and K. W. Lehnert, *Nat. Phys.* **17**, 322 (2021).
- [21] E. A. Wollack, A. Y. Cleland, R. G. Gruenke, Z. Wang, P. Arrangoiz-Arriola, and A. H. Safavi-Naeini, *Nature* **604**, 463 (2022).
- [22] R. N. Patel, T. P. McKenna, Z. Wang, J. D. Witmer, W. Jiang, R. Van Laer, C. J. Sarabalis, and A. H. Safavi-Naeini, *Phys. Rev. Lett.* **127**, 133602 (2021).
- [23] G.ENZIAN, L. Freisem, J. J. Price, A. Ø. Svela, J. Clarke, B. Shajilal, J. Janousek, B. C. Buchler, P. K. Lam, and M. R. Vanner, *Phys. Rev. Lett.* **127**, 243601 (2021).
- [24] W. J. Munro, K. Nemoto, G. J. Milburn, and S. L. Braunstein, *Phys. Rev. A* **66**, 023819 (2002).
- [25] J. Joo, W. J. Munro, and T. P. Spiller, *Phys. Rev. Lett.* **107**, 083601 (2011).
- [26] K. Jacobs, R. Balu, and J. D. Teufel, *Phys. Rev. A* **96**, 023858 (2017).
- [27] N. Sangouard, C. Simon, N. Gisin, J. Laurat, R. Tualle-Brouiri, and P. Grangier, *J. Opt. Soc. Am. B* **27**, A137 (2010).
- [28] J. B. Brask, I. Rigas, E. S. Polzik, U. L. Andersen, and A. S. Sørensen, *Phys. Rev. Lett.* **105**, 160501 (2010).
- [29] Z. Leghtas, G. Kirchmair, B. Vlastakis, R. J. Schoelkopf, M. H. Devoret, and M. Mirrahimi, *Phys. Rev. Lett.* **111**, 120501 (2013).
- [30] C. Chamberland, K. Noh, P. Arrangoiz-Arriola, E. T. Campbell, C. T. Hann, J. Iverson, H. Putterman, T. C. Bohdanowicz, S. T. Flammia, A. Keller, G. Refael, J. Preskill, L. Jiang, A. H. Safavi-Naeini, O. Painter, and F. G. S. L. Brandão, *PRX Quantum* **3**, 010329 (2022).
- [31] S. Bose, K. Jacobs, and P. L. Knight, *Phys. Rev. A* **59**, 3204 (1999).

- [32] S. Bose, K. Jacobs, and P. L. Knight, *Phys. Rev. A* **56**, 4175 (1997).
- [33] W. Marshall, C. Simon, R. Penrose, and D. Bouwmeester, *Phys. Rev. Lett.* **91**, 130401 (2003).
- [34] U. Akram, W. P. Bowen, and G. J. Milburn, *New J. Phys.* **15**, 093007 (2013).
- [35] H. Zhan, G. Li, and H. Tan, *Phys. Rev. A* **101**, 063834 (2020).
- [36] I. Shomroni, L. Qiu, and T. J. Kippenberg, *Phys. Rev. A* **101**, 033812 (2020).
- [37] A. C. Pflanze, O. Romero-Isart, and J. I. Cirac, *Phys. Rev. A* **88**, 033804 (2013).
- [38] Z.-Q. Yin, T. Li, X. Zhang, and L. M. Duan, *Phys. Rev. A* **88**, 033614 (2013).
- [39] U. B. Hoff, J. Kollath-Bönig, J. S. Neergaard-Nielsen, and U. L. Andersen, *Phys. Rev. Lett.* **117**, 143601 (2016).
- [40] R. Y. Teh, S. Kiesewetter, P. D. Drummond, and M. D. Reid, *Phys. Rev. A* **98**, 063814 (2018).
- [41] W. Ge and M. S. Zubairy, *Phys. Rev. A* **91**, 013842 (2015).
- [42] J.-Q. Liao and L. Tian, *Phys. Rev. Lett.* **116**, 163602 (2016).
- [43] G. A. Brawley, M. R. Vanner, P. E. Larsen, S. Schmid, A. Boisen, and W. P. Bowen, *Nat. Commun.* **7**, 10988 (2016).
- [44] E. J. Davis, Z. Wang, A. H. Safavi-Naeini, and M. H. Schleier-Smith, *Phys. Rev. Lett.* **121**, 123602 (2018).
- [45] J. Clarke and M. R. Vanner, *Quantum Sci. Technol.* **4**, 014003 (2019).
- [46] H. Tan, F. Bariani, G. Li, and P. Meystre, *Phys. Rev. A* **88**, 023817 (2013).
- [47] M. Asjad and D. Vitali, *J. Phys. B* **47**, 045502 (2014).
- [48] M. Brunelli, O. Houhou, D. W. Moore, A. Nunnenkamp, M. Paternostro, and A. Ferraro, *Phys. Rev. A* **98**, 063801 (2018).
- [49] M. Brunelli and O. Houhou, *Phys. Rev. A* **100**, 013831 (2019).
- [50] J. D. Thompson, B. M. Zwickl, A. M. Jayich, F. Marquardt, S. M. Girvin, and J. G. E. Harris, *Nature* **452**, 72 (2008).
- [51] C. Doolin, B. D. Hauer, P. H. Kim, A. J. R. MacDonald, H. Ramp, and J. P. Davis, *Phys. Rev. A* **89**, 053838 (2014).
- [52] M. S. Kim and V. Bužek, *Phys. Rev. A* **46**, 4239 (1992).
- [53] See Supplementary Material for expanded information about cat states and detailed calculations for our protocol, which includes Refs. [54–67].
- [54] V. V. Dodonov, I. A. Malkin, and V. I. Man'ko, *Physica* **72**, 597 (1974).
- [55] R. J. Glauber, *Phys. Rev.* **131**, 2766 (1963).
- [56] E. Wigner, *Phys. Rev.* **40**, 749 (1932).
- [57] C. C. Gerry and P. L. Knight, *Am. J. Phys.* **65**, 964 (1997).
- [58] A. Kenfack and K. Życzkowski, *J. Opt. B* **6**, 396 (2004).
- [59] A. Grimm, N. E. Frattini, S. Puri, S. O. Mundhada, S. Touzard, M. Mirrahimi, S. M. Girvin, S. Shankar, and M. H. Devoret, *Nature* **584**, 205 (2020).
- [60] M. Mirrahimi, Z. Leghtas, V. V. Albert, S. Touzard, R. J. Schoelkopf, L. Jiang, and M. H. Devoret, *New J. Phys.* **16**, 045014 (2014).
- [61] J. M. Luttinger and W. Kohn, *Phys. Rev.* **97**, 869 (1955).
- [62] J. R. Schrieffer and P. A. Wolff, *Phys. Rev.* **149**, 491 (1966).
- [63] S. Nakajima, *Prog. Theor. Phys.* **20**, 948 (1958).
- [64] R. Zwanzig, *J. Chem. Phys.* **33**, 1338 (1960).
- [65] R. Zwanzig, *Physica* **30**, 1109 (1964).
- [66] N. Lörch, *Laser theory for quantum optomechanics*, Ph.D. thesis, Gottfried Wilhelm Leibniz Universität Hannover (2015).
- [67] R. Gautier, A. Sarlette, and M. Mirrahimi, *PRX Quantum* **3**, 020339 (2022).
- [68] J. D. P. Machado and Y. M. Blanter, *Phys. Rev. A* **94**, 063835 (2016).
- [69] A. Nunnenkamp, K. Børkje, and S. M. Girvin, *Phys. Rev. Lett.* **107**, 063602 (2011).
- [70] I. Wilson-Rae, N. Nooshi, J. Dobrindt, T. J. Kippenberg, and W. Zwerger, *New J. Phys.* **10**, 095007 (2008).
- [71] J. D. Teufel, D. Li, M. S. Allman, K. Cicak, A. J. Sirois, J. D. Whittaker, and R. W. Simmonds, *Nature* **471**, 204 (2011).
- [72] J. Chan, A. H. Safavi-Naeini, J. T. Hill, S. Meenehan, and O. Painter, *Appl. Phys. Lett.* **101**, 081115 (2012).
- [73] A. Bozkurt, C. Joshi, and M. Mirhosseini, *Opt. Express* **30**, 12378 (2022).
- [74] M. Reagor, H. Paik, G. Catelani, L. Sun, C. Axline, E. Holland, I. M. Pop, N. A. Masluk, T. Brecht, L. Frunzio, M. H. Devoret, L. Glazman, and R. J. Schoelkopf, *Appl. Phys. Lett.* **102**, 192604 (2013).
- [75] B. D. Hauer, K. Cicak, F. Lecocq, R. W. Simmonds, J. Aumentado, and J. D. Teufel, *Conference on Lasers and Electro-Optics , STu2H.2* (2021).
- [76] R. D. Delaney, A. P. Reed, R. W. Andrews, and K. W. Lehnert, *Phys. Rev. Lett.* **123**, 183603 (2019).
- [77] A. L. Grimsmo, J. Combes, and B. Q. Baragiola, *Phys. Rev. X* **10**, 011058 (2020).